Application of the Genetic Algorithm Joint with the Powell Method to Nonlinear Least-Squares Fitting of Powder EPR Spectra

Tomasz Spałek,† Piotr Pietrzyk,† and Zbigniew Sojka*,†,‡

Faculty of Chemistry, Jagiellonian University, Ingardena 3, 30-060 Cracow, Poland, and Regional Laboratory of Physicochemical Analyses and Structural Research, Ingardena 3, 30-060 Cracow, Poland

Received April 22, 2004

The application of the stochastic genetic algorithm (GA) in conjunction with the deterministic Powell search to analysis of the multicomponent powder EPR spectra based on computer simulation is described. This approach allows for automated extraction of the magnetic parameters and relative abundances of the component signals, from the nonlinear least-squares fitting of experimental spectra, with minimum outside intervention. The efficiency and robustness of GA alone and its hybrid variant with the Powell method was demonstrated using complex simulated and real EPR data sets. The unique capacity of the genetic algorithm for locating global minima, subsequently refined by the Powell method, allowed for successful fitting of the spectra. The influence of the population size, mutation, and crossover rates on the performance of GA was also investigated.

1. INTRODUCTION

Electron paramagnetic resonance (EPR) also known as electron spin resonance (ESR) spectroscopy is a powerful tool for characterizing chemical species that contain unpaired electrons such as radicals, transition metal ions, or defect centers. The extreme sensitivity and information content of the spectra are probably the most acknowledged advantages that contribute to large applications of EPR spectroscopy in chemistry, solid-state physics, and molecular biology. With the advent of the spin Hamiltonian concept[1] in the beginnings, the primary goal in much of EPR practice was a direct measurement of the spin Hamiltonian parameters from the positions of spectral lines in the magnetic field. Over the past two decades the focus has shifted toward computer simulation, the only method suitable for accurately extracting the EPR parameters, especially in the case of randomly oriented powders, glasses, or frozen solutions.[2] Because usually the number of parameters to be optimized is large, single simulations are of rather limited practical value, and automated fitting has become an indispensable component in any proficient analysis of the powder EPR spectrum.[2,3]

The complexity of EPR powder spectra imposes several restrictions on apposite optimization methods for searching the spin Hamiltonian parameter space H_p, which should possess the following characteristics: (*i*) do not require or minimize any derivative information, (*ii*) be resistant to local minima, (*iii*) be effective in very nonlinear problems, and (*iv*) be sparing in use of target function evaluations and not affected adversely when it is large.[4] These requirements disfavor nonlinear least squares approaches that require derivative information, despite their advantages discussed elsewhere,[5] approving direct search methods,[3,4] downhill simplex algorithms,[6] or global techniques such as simulated annealing[7] or genetic algorithms,[8,9] to tackle difficult optimization problems with many local optima.

The genetic algorithm is an optimization method employing a probabilistic, nonlocal search heuristics that simulates natural evolution. The major strength of GA is the ability to explore and exploit a large parameter space with no initial guesses and derivative information, without trapping in local minima. However, GA exhibits a distinct drawback, the true minium, i.e., the best solution, is rarely reached albeit it may be closely approached.[8,9] Therefore, regardless of the quality of the results obtained with the genetic algorithm, traditional minimum search techniques such as Gauss−Newton[10] and Hooke and Jeeves[11] may be used as complementary second step measures to refine the ultimate results. Despite the wide range of applications of GA to many chemical problems,[12,13] optimization of the powder EPR spectra remains still an unexplored field of its potential advantage. To our knowledge, except for our preliminary work on static randomly oriented spectra,[14] only a paper by Filipic and Strancar[15] reported on the application of GA to analysis of the EPR spectra of motionally restricted fluid solutions.

2. THEORETICAL OUTLINE

2.1. Simulation of Powder EPR spectra. Static EPR spectra of randomly oriented isolated paramagnets with $S = {}^1/_2$ and $I > 0$ are described by the spin Hamiltonian, typically written in the form

$$H = \beta_e \boldsymbol{S}\cdot\boldsymbol{g}\cdot\boldsymbol{B} + \Sigma\, \boldsymbol{S}\cdot\boldsymbol{A}_i\cdot\boldsymbol{I}_i \qquad (1)$$

where the subsequent terms represent electronic Zeeman and hyperfine interactions, respectively. In the case of randomly oriented systems usually the nuclear Zeeman, $g_N\beta_N\boldsymbol{IB}$, and in many situations also the quadruple, $\boldsymbol{I}\cdot\boldsymbol{Q}\cdot\boldsymbol{I}$, terms (for $I \geq 1$) are neglected as they usually do not contribute seemingly to the final shape of most of the powder EPR spectra.[3]

* Corresponding author phone: +48 12 663 22 95; fax: +48 12 634 05 15; e-mail: sojka@chemia.uj.edu.pl.

† Faculty of Chemistry.

‡ Regional Laboratory of Physicochemical Analyses and Structural Research.

10.1021/ci049863s CCC: $30.25
Published on Web 11/24/2004

The parameters of the spin Hamiltonian to be determined experimentally, usually referred to as $\boldsymbol{g}$ and $\boldsymbol{A}$ tensors etc., fully describe all EPR lines and their relative intensities and convey meaningful molecular information about the investigated system. The powder spectrum can be considered as a superposition of single-crystal EPR signals computed for a large number of orientations (θ, ϕ) of the external magnetic field $\boldsymbol{B}$ over the unit sphere weighted in proportion of $\sin\theta d\theta d\phi$. The resultant pattern can be expressed as follows[16]

$$Y(B,\nu) = C\int_{\theta=0}^{\pi/2}\int_{\varphi=0}^{2\pi}\sum_i P(i,\theta,\varphi,\nu) f(B - B_o[\nu],\sigma_B)\mathrm{d}\cos\theta\mathrm{d}\varphi \quad (2)$$

where $P(i,\theta,\phi,\nu)$ is the transition probability, $f(B - B_0[\nu], \sigma_B)$ is the line shape function (usually assuming a Gaussian or Lorentzian form), and C is a constant that incorporates all instrumental parameters. The most common line width model is based on the classic angular variation formula

$$\sigma_B = (\sigma_x^2(B)\cos^2\phi\sin^2\theta + \sigma_y^2(B)\sin^2\phi\sin^2\theta + \sigma_z^2(B)\cos^2\theta)^{1/2} \quad (3)$$

where $\sigma_q(B)$, $q = x, y, z$, are the input line width values.

Because the line positions generally are not strictly linear in any of the magnetic parameters, and the latter occur intermingled in the energy expressions, the analysis of EPR spectra appears to generally be nontrivial. The problems proliferate when several paramagnetic species occur simultaneously, giving rise to multicomponent EPR spectra

$$Y(B,\nu) = a_1Y_1(B,\nu) + a_2Y_2(B,\nu) + ...a_cY_c(B,\nu) \quad (4)$$

In such cases partially resolved and overlapped signals, often encountered in practice,[17] may severely impede detection of the individual EPR features, making determination of the spin Hamiltonian parameters difficult. As a result, computer simulation combined with fitting appears to be practically the only way of reliable analysis of the experimental powder EPR spectra. A large number of suitable programs of various sophistication levels have been developed in past decades for this purpose.[2,3,5,18]

2.2. Optimization Procedure. Mathematically the experimental and calculated EPR spectra constitute two sets of discrete data points $\boldsymbol{Y} = (Y_1.....Y_n)$ and $\boldsymbol{y} = (y_1.....y_n)$, respectively. If $\boldsymbol{P}$ represents all input parameters needed to fully describe the spectrum, then $\boldsymbol{y} = \mathrm{f}(\boldsymbol{P})$. The simulation problem consists of finding such $\boldsymbol{P}$ to make $\boldsymbol{y} = \mathrm{f}(\boldsymbol{P})$ as close as possible to $\boldsymbol{Y}$.[4] The quality of the fit gauged by an error function $E(\boldsymbol{y},\boldsymbol{Y},\boldsymbol{w})$ is usually characterized by the sum of the weighted square deviations between the calculated and experimental spectra, normalized by the noise variance and the number of data points.[19] Some other criterions have also been reported.[3] Thus, an automated determination of the EPR parameters is a multivariate optimization problem of finding the minimum of

$$E(\mathrm{f}(\boldsymbol{P}),\boldsymbol{Y},\boldsymbol{w}) = 1/N\Sigma w_i(Y_i - s_iy_i)^2 \quad (5)$$

where w_i and s_i are the peak weighting and spectra scaling factors, respectively, and N is the number of data points. In the case of noiseless synthetic spectra by taking $w_i = 1$ the $E(\boldsymbol{y},\boldsymbol{Y},\boldsymbol{w})$ function is equivalent to the root-mean-square error (RMS), whereas for noisy spectra with $w_i = \sigma_i^2$ it corresponds to χ^2.

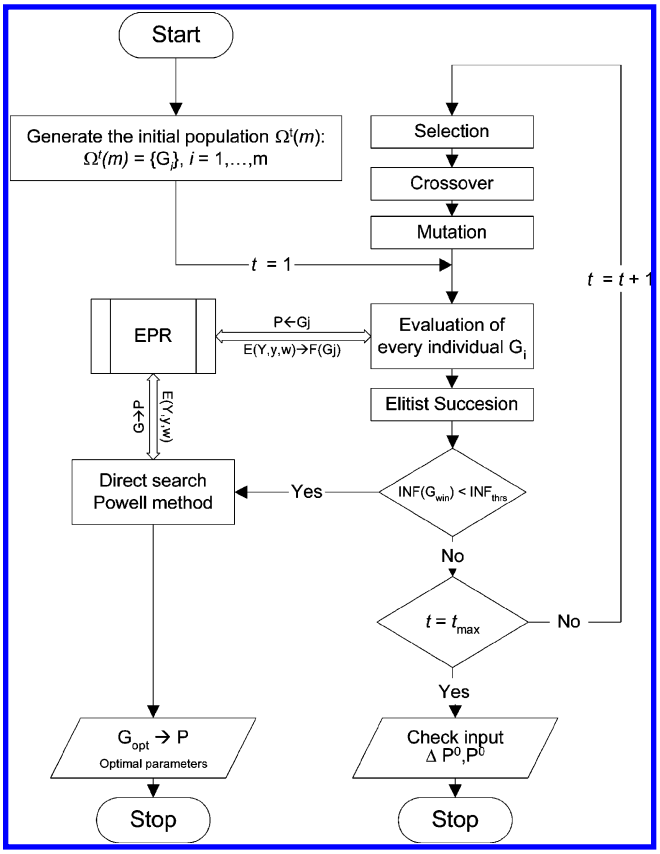

Figure 1. Flowchart of the hybrid optimization method for automatic analysis of powder EPR spectra based on the combination of a genetic algorithm search with Powell refinement. The double arrow ⟺ indicates a communication with the EPR module.

The success of the traditional local refinement methods strongly depends on the starting point[10,11] and is rapidly restrained with increasing the number of the parameters. They can also be easily trapped in local valleys and thereby often fail to locate the global minimum. Thus, a promising solution of such problems can be provided by hybridization of direct search methods with global genetic algorithms.

2.3. Adapting GA to Automated Analysis of EPR Spectra. Many different variants of evolutionary algorithms have been developed.[20−22] Although the underlying principles are relatively simple, those algorithms have proven themselves as robust and powerful search tools, owing to their remarkable flexibility and adaptability to a given task. Hereafter a brief description focuses on how to tailor a genetic algorithm to automate the process of determining the spin Hamiltonian parameters from powder EPR spectra via computer simulation.

For optimization of multicomponent EPR spectra we have implemented into a simulation program EPRsim32 (vide infra) an evolution algorithm described elsewhere.[23] The structure of the algorithm is outlined in a flowchart shown in Figure 1, while the notation used is explained in Table 1. To define properly the GA machinery in a particular application, one should provide the size m of the initial population $\Omega^t(m)$ of individuals G_i, $i = 1,..., m$, the coding method, the fitness index $F(G_i)$ of each individual, and the

Table 1. Notation Used in the Flowchart of GA-Based Optimization of EPR Spectra

notation	definition
$\boldsymbol{Y}, \boldsymbol{y}$	experimental and calculated EPR spectra
$\boldsymbol{P} = \{p_i\}$	full set simulation parameters p_i
$E(\mathbf{y},\boldsymbol{Y},\boldsymbol{w})$	error (objective) function
$\Omega^t(m)$	tth population of the size m of individuals G_i
$G_i = \{X_1, X_2,.., X_c\}$	an individual i composed of c chromosomes X_j corresponding to component EPR signals contributing to total spectrum
$X_j[n \times 1] = [x_1, x_2, ..., x_n]$ $x_i \epsilon [-1, 1]$	a string of chromosome with n genes corresponding to n parameters to be optimized
$F(G_i)$	fitness index of an ith individual
G_{win}	the fittest individual in current population t
G_{opt}	the fittest individual of ultimate GA-Powell optimization
G_i'	an individual i complemented by its fitness index $F(G_i)$
P°, ΔP°	strings of starting parameters and their uncertainties c
$INF(G_i)$	intimate neighborhood impact factor evaluated for an individual G_i
INF_{thrs}	threshold value of INF
t_{max}	maximum number of generations

formulation of genetic operators. It invokes four data processing steps: representation, selection, recombination (crossover), and mutation.

In the adopted representation, a full set of the current input variables $\boldsymbol{P}$ to be optimized was encoded into an individual $G_i = \{X_1, X_2,..., X_c\}$, composed of c chromosomes X_j corresponding to the particular components $Y_j(B, v)$ of the EPR spectrum. The polychromosomic individuals were preferred over the usual monochromosomic species, since they reflect better the structure of the optimization subject (multicomponent spectrum). Each chromosome is a string of the form $X_j = \{x_1^j, x_2^j,..., x_n^j\}$, where x_n^j stands for the genes, the number of which is equal to the number of optimizable parameters n of the component signal j. In the applied representation the genes are coded as 32-bit floating point numbers from the $[-1, 1]$ range. The adjustable simulation parameters p_{ij}, i.e., the spin Hamiltonian parameters, line widths $\sigma_q(B)$, and the relative contributions a of the component signals $Y_j(B, v)$ of the resultant spectrum are related to the corresponding genes x_i^j in the following way: $p_{ij} = x_i^j \Delta p_{ij}^o + p_{ij}^o$, where p_{ij}^o corresponds to their initial values and Δp_{ij}^o to the assumed uncertainty intervals ($\Delta p^o = [p_{min}, p_{max}]$). The overall structure of such representation is shown below in more detail.

Scheme 1. The Relationship between the Genotype and Phenotype Spaces[a]

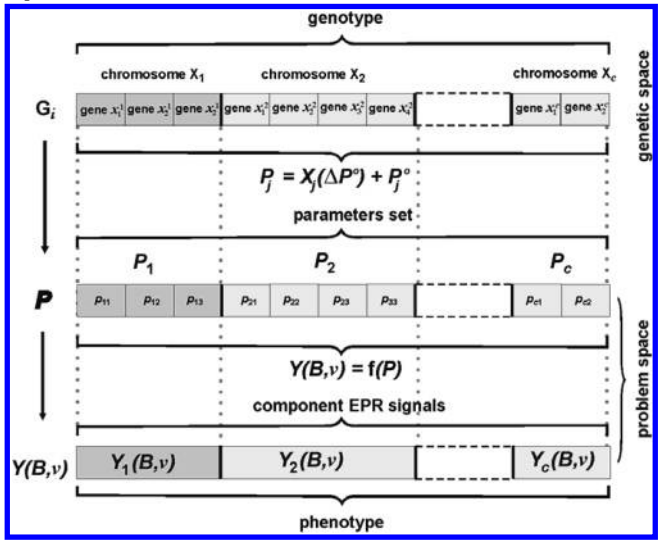

[a]The polychromosomic genotype of an individual G_i is mapped into the corresponding parameter space $P = \{P_j\}$, and next P is used for simulation of the EPR spectrum $Y_j(B, v) = F(P)$.

One of the advantages of floating point representation consists of retaining the proximity between two points in both spaces: the representation and the problem one.[23] Despite the lack of well established theoretical justification for using real-coded genes, the floating point representation appeares to be faster and easier to implement and provides higher precision than its binary analogue, particularly in large domains where the binary strings would be prohibitively long.[24]

The chromosome X_j containing the information about the all adjustable parameters of the component signal j, can be regarded as the basal one for a descendant chromosome X_j': $[k \times 1]$, $k < c$, which collects k simulation parameters P_j' that are currently optimized. The X_j and X_j' strings are mutually related through user defined selection vector $\mathbf{T}[c \times 1]$, which allocates the parameters for the adjustment in a given simulation run, following the scheme

Scheme 2. Selection Vector $\mathbf{T}[c \times 1]$ Relating k Currently Optimized Parameters P' and c Adjustable Parameters P

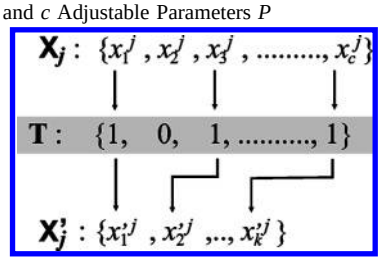

Such operation allows for reduction of the number of variables, by fixing those parameters that are supposed to be optimal or currently kept constant for certain reasons (latent variables). By analogy to the gene-parameter relationship, the information contained in the chromosome X_j can be translated into the parameter space using the relation

$$P_j = X_j(\Delta P_j^o) + P_j^o \qquad (6)$$

where $P_j^o = \{p_{1j}^o, p_{2j}^o, p_{3j}^o ..... p_{nj}^o\}$ and $\Delta P_j^o = \{\Delta p_{1j}^o, \Delta p_{2j}^o, \Delta p_{3j}^o ..... \Delta p_{nj}^o\}$ are the strings of the starting parameters and their uncertainties of the component signal j, respectively.

A basal set of the simulation parameters for each component signal j is obtained by combining the string P_j' of the adjustable parameters $\{\boldsymbol{g}$ and $\boldsymbol{A}$ tensors, $\sigma_q(B)$, a_j, ...$\}$ with a string Q_j' of the associated parametric variables $\{S, I, \theta, \phi, h, ...\}$, containing complementary information about the

electronic and nuclear spin values, θ and ϕ angles, the number simulation points h, etc.

In the case of nuclei of various isotopic composition like molybdenum, the P_j and Q_j strings are associated with the fundamental isotopomer of the component j, i.e., that with the largest number of the magnetic parameters. They have to be complemented by related $P_j(i)$ and $Q_j(i)$ strings accounting for all descendant isotopomers i, through appropriate modification of the reliant parameters (e.g., $A_{pq}(i) = g_n(i)/g_n A_{pq}$ where g_n are the tabulated nuclear g factors) and suitable amendment of the parametric variables Q_j. For instance, in the case of O-17 enriched superoxide radical with nonequivalent nuclei there are four isotopomers $^{17}O^{17}O$, $^{17}O^{16}O$, $^{16}O^{17}O$, $^{16}O^{16}O$, and the $^{17}O^{17}O$ can be taken as a fundamental one. The relative abundances of the descendant isotopomers can either be calculated a priori,[25] from the known isotopic compositions or taken as another adjustable parameter inserted into the P_j string. The complete set P_j of the parameters required for simulation of a given component signal j is then defined by an ensemble of P_j, $P_j(i)$ and Q_j, $Q_j(i)$ strings of all isotopomers. Obviously, only the parameters of the fundamental isotopomers (P_j) have to be optimized, all dependent parameters $P_j(i)$ of the remaining isotopomers, needed for simulation, are derived from the P_j values. Finally, for a multicomponent EPR spectrum the full set $\boldsymbol{P}$ of the simulation parameters can be created by simple aggregation of the strings P_j, of all partaking components, $\boldsymbol{P} = \{P_j\}$, $j = 1, c$.

In such an approach the ensemble of the basal chromosomes X constituting an individual G_i can be identified with a genotype corresponding to the all simulation parameters $G_i \rightarrow \boldsymbol{P}$. The associated phenotype is then constituted by the associated simulated EPR spectrum calculated with those parameters (the genotype). Both spaces are linked together by translation function (the simulation) converting the genotype space into the phenotype space ($\boldsymbol{Y} = f(\boldsymbol{P}(G_i))$, which is in turn compared with the environment (the experimental spectrum $\boldsymbol{y}$). The error function $E(\boldsymbol{Y},\boldsymbol{y},\boldsymbol{w})$ is used as a fitness criterion to be minimized (Scheme 1).

The flowchart shown in Figure 1 explains the interplay between the GA optimization and the EPR simulation program. At the beginning an initial population $\Omega^1(m)$ of the individuals G_i (potential solutions) has to be created. Each gene of an individual G_i encodes a preliminary value of the associated adjustable parameter, selected at random from the assumed uncertainty range. The individuals are next evaluated by calling the simulation program EPR and the calculated fitness indexes $F(G_i)$ are associated with the G_i strings ($G_i \rightarrow G_i'$). The fitness index composed of two numbers, a root-mean-square error (or χ^2) and the value of an intimate neighborhood impact factor $F(G_i) = \{E(\boldsymbol{Y},\boldsymbol{y},\boldsymbol{w}), \mathrm{INF}(\boldsymbol{Y},\boldsymbol{y},\epsilon)\}$, was used for scoring the individuals. The INF$(\boldsymbol{Y},\boldsymbol{y},\epsilon)$ gauges the fraction of the simulated data points which are located within a user defined envelope of the experimental spectrum. The widths of this envelope are determined by an ϵ value, which usually is dictated by the noise level (vide infra).[14] The intimate neighborhood impact factor provides a concise and stabile measure of the global optimization successfulness. The value of INF$(\boldsymbol{Y},\boldsymbol{y},\epsilon)$ is used as a criterion for switching from GA to Powell search, whereas $E(\boldsymbol{Y},\boldsymbol{y},\boldsymbol{w})$ is an actual subject of the optimization process. Determining the fitness of an individual is computationally the most demanding step of the GA optimization since it requires numerical simulation of the EPR spectrum. Actually the genetic algorithm makes use of a modified fitness function $E'(\boldsymbol{Y}(G_i),\boldsymbol{y},\boldsymbol{w}) = E(\boldsymbol{Y}(G_o),\boldsymbol{y},\boldsymbol{w}) - E(\boldsymbol{Y}(G_i),\boldsymbol{y},\boldsymbol{w})$, where $E(\boldsymbol{Y}(G_o),\boldsymbol{y},\boldsymbol{w})$ is the fitness of the worst adapted individual, i.e., that of the highest $E(\boldsymbol{Y},\boldsymbol{y},\boldsymbol{w})$ value in the initial population.

Based on the $E'(\boldsymbol{Y},\boldsymbol{y},\boldsymbol{w})$ values the G_i' individuals are ranked according to their merit, and the fittest individual (the winner) is duplicated and saved as G_{win}. If at least 95% of the calculated spectral points (an arbitrary threshold value of the INF criterion) appear within the envelope of the intimate neighborhood, i.e., $\mathrm{INF}(G_{win}) > \mathrm{INF}_{thrs}$, the global optimization is considered to be accomplished successfully, and the set of the parameters connected with G_{win} is used as a starting point for direct search refinement. Thus, at this stage the GA optimization is tantamount with the Monte Carlo search for an advantageous starting point, with the number of trials equal to the population size.

In the case when the G_{win} individual fails the INF test ($\mathrm{INF}(G_{win}) < \mathrm{INF}_{thrs}$), the population is subjected to the reproduction process using the genetic operations in the sequence indicated in Figure 1. The selection operation chooses the best individuals of the current population for reproduction in the next generation. A fitness proportionate selection (roulette wheel)[26] along with an elitist succession was applied to produce the offspring. In this approach the reproduction probability $W_t(G_i)$ of an individual G_i is proportional to its $E'(\boldsymbol{Y}(G_i),\boldsymbol{y},\boldsymbol{w})$ value, normalized over the whole population:

$$W_t(G_i) = \frac{E'(\boldsymbol{Y}(G_i),\mathbf{y},\mathbf{w})}{\sum_{i=1}^{m} E'(\boldsymbol{Y}(G_i),\mathbf{y},\mathbf{w})} \tag{7}$$

To ensure that good solutions are not lost regularly, a fraction r of the top individuals from the parent population is placed in the next generation (from which r worst individuals has been removed) without any changes. The actual fraction of retention defines the selection pressure. When size of the elite is large from one generation to another, the algorithm can exhibit narrow population diversity. On the other hand, a small fraction might not retain enough of the desirable characteristics to overcome convergence problems.

The descendent individuals are produced through the operations of crossover and mutation. A uniform crossover operator was used for this purpose. Its action consists of arithmetic averaging of the parental chromosomes X_1 and X_2 (appropriate for the floating-point representation) and can be described in the following way

$$\begin{aligned} X_1^{\,new} &= X_1^{\,old} + g(X_2^{\,old} - X_1^{\,old}) \\ X_2^{\,new} &= X_2^{\,old} + g(X_1^{\,old} - X_2^{\,old}) \end{aligned} \tag{8}$$

where g is a random number with uniform distribution in the [0, 1] interval. Such choice has a big advantage, because new chromosome values will be automatically inside their definition ranges.

In the last step the chromosomes undergo the mutation operation. This operation is helpful in preventing premature convergence and ensuring the diversity of the individuals. A probability variable controls the mutation process and

usually has a small value inversely proportional to the number of genes.[27] The floating point representation suggests the usage of a nonuniform mutation described by the following fluctuation function

$$\Delta(\tau,z) = z(1 - r^{(1-\tau/t_{\max})^b}) \quad (9)$$

where τ stands for the evolution time, r is a random number from the [0, 1] range, z limits the maximum variation of the given gene, whereas b describes the system nonuniformity.[23] The resulting population is sorted by fitness, and the top m individuals are retained for the next generation $\Omega^{t+1}(m)$. The iterative cycles (generations) are repeated until the optimization or stopping criterium ($t \leq t_{\max}$) is fulfilled.

3. EPR SIMULATION PROGRAM

Simulated test spectra were obtained using an EPRsim32 program written in Microsoft visual C^{++} 6.0 using the MFC library. The program has building blocks based on the approach described above. The program runs under Microsoft Windows with full 32 coding. It has a user-friendly interface based on mouse-driven access to pull-down menus and dialogue boxes. The simulated spectrum can be saved as an ASCII file, and hardcopy is available using any output device supported by Microsoft Windows. The interactive graphics for monitoring of the simulation progress, visualization of data in conjunction with the experimental spectrum, versatile tools for peak picking and line shape analysis, interactive stick diagram generation for provisional assessment of $\boldsymbol{g}$, and hyperfine splittings are available. A short calculation time along with the possibility of manual stepping of variables provides users with a better understanding of spectral response to changes of the parameters, in nearly-real time.

The program allows for analysis of the static randomly oriented continuous wave multicomponent EPR spectra (including isotopomers) with $S = {}^1/_2$ and coincident principal axes. The second-order perturbation formula was used to calculate resonance fields along with the powder averaged transition probabilities $\langle g_1^2/g \rangle$ for evaluation of the line intensities.[3] The line shape can be either Lorentzian, Gaussian, or mixed, and the orientation dependent line width can be used. Because of extensive calling of the simulation module, evaluation of the GA performance and spectra optimization are quite time-consuming. Thus, using of the closed form perturbation formula instead of demanding energy matrix diagonalization helped us to speed up this process essentially.

4. DATA SETS

The performance of the GA-based optimization algorithm was tested using synthetic and real data sets of increasing complexity, corresponding to typical spectroscopic properties of transition metal ions exchanged into ZSM-5 zeolites, we have encountered in our studies. A rather straightforward test spectrum $\mathbf{T_1}$ with 17 adjustable parameters was composed of three superimposed signals ($\mathbf{S_1}$-1, $\mathbf{S_1}$-2, $\mathbf{S_1}$-3) that refer to various types of copper intrazeolite complexes (the axial signal $\mathbf{S_1}$-1, with $g_{\|} > g_{\perp}$ and $A_{\|} > A_{\perp}$, corresponds to copper in a square pyramid) and the signal $\mathbf{S_1}$-2, with $g_{\perp} > g_{\|}$ and $A_{\|} > A_{\perp}$, to a trigonal bipyramid coordination, whereas the isotropic signal $\mathbf{S_1}$-3 to a hexaaqua complex averaged by tumbling. These are three generic species of divalent copper entrapped in zeolites, depending on the dehydration state. A test spectrum $\mathbf{T_2}$ having 26 adjustable parameters was composed of three orthorhombic ($\mathbf{S_2}$-1, $\mathbf{S_2}$-2, $\mathbf{S_2}$-3) and one axial signal ($\mathbf{S_2}$-4), all without the hyperfine structure, and the $\boldsymbol{g}$ tensor values that are characteristic of mono-, di-, tri-, and tetracarbonyl complexes of nickel in ZSM-5. A test spectrum $\mathbf{T_3}$ with 21 parameters to be optimized was produced by three largely overlapped axial signals ($\mathbf{S_3}$-1, $\mathbf{S_3}$-2, $\mathbf{S_3}$-3) with pronounced hyperfine structure due to speciation of low spin tricarbonyl cobalt intrazeolite adducts. The $\mathbf{T_1}$, $\mathbf{T_2}$, and $\mathbf{T_3}$ spectra along with the component signals are shown in Figure 2a, b, c, and the corresponding parameters are collected in Table 2.

The experimental EPR spectrum $\mathbf{T_4}$ of $\{(CO)_n Ni\}^9$/ZSM-5 (Figure 2d) was recorded on a Bruker ELEXYS spectrometer, working at X-band with a rectangular TE_{102} cavity and 100 kHz modulation. Since any distortion of the experimental spectra will reduce the fidelity of the simulation, our analysis is restricted to spectra for which the modulation distortions are small, the saturation can be neglected, and the slow passage condition is fulfilled.

5. OPTIMIZATION OF THE GA PARAMETERS

The operational efficiency of a genetic algorithm is intimately controlled by the values of such parameters as the population size, the crossover and mutation probabilities, the decay factor, and the percentage of elitist retention, which control various aspects of the algorithm in a given implementation. There is no sound theoretical basis for a priori assignment of their values, albeit some general hints are available.[8,22] Thus, to determine such setting for our application, parametric sensitivity tests were performed. Because of the stochastic nature of GA, sensible conclusions can only be based on the average performance over several runs. Therefore, to obtain reliable results and minimize the influence of the initial population 10−20 independent trials with a randomly varying starting population were performed in all testing experiments.

5.1. Establishing of the Crossover and Mutation Rates. The sensitivity of the GA-based fitting of EPR spectra to the probabilities of crossover and mutation was examined using the $\mathbf{T_1}$, $\mathbf{T_2}$, and $\mathbf{T_3}$ data set. Optimization of those parameters is an important issue since the relative probabilities of the crossover and mutation determine the balance between the exploitation and exploration moves that are crucial for performance of the algorithm. The probability of the crossover (p_{crs}) was paced in the range [0, 1] with a 0.1 step, whereas the mutation probability (p_{mut}) was paced in the range [0, 0.1] with a 0.01 step. As a result a grid of 121 data points was created, and the GA optimization, with a population of the size $m = 100$, was successively iterated over the generations for each pair of the values. The results of the parametric sensitivity study, averaged over three independent runs, are summarized in the form of operator performance maps shown in Figure 3, where log of the convergence efficiency, gauged by the number of simulations required to achieve the INF threshold of 95%, is drawn as a function of the crossover and mutation probabilities. From the inspection of Figure 3 it is clear that an increase of the crossover rate tends to enhance the performance of GA for

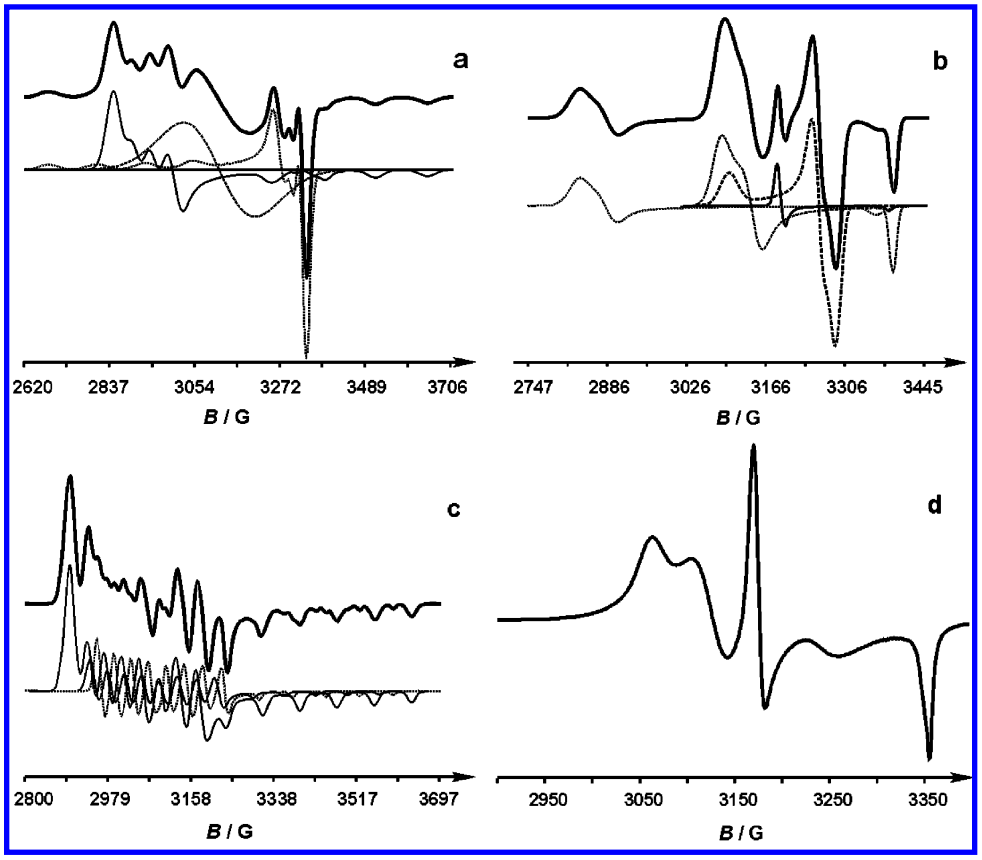

Figure 2. Synthetic EPR test spectra along with the component signals (a) $\mathbf{T_1}$, (b) $\mathbf{T_2}$, (c) $\mathbf{T_3}$, and (d) experimental spectrum $\mathbf{T_4}$ of nickel carbonyl complexes in ZSM-5.

Table 2. EPR Parameters of the $\mathbf{T_1}$, $\mathbf{T_2}$, and $\mathbf{T_3}$ Test Spectra Used for Evaluation of Genetic Algorithm Performance

spectrum	***g***-tensor	***A***-tensor/G	line widths/G
T_1			
S_1-1	$g_{\|\|} = 2.37 \pm 0.126$, $g_\perp = 2.06 \pm 0.126$	$A_{\|\|} = 121 \pm 25$ $A_\perp = 20 \pm 8$	$\delta_{\|\|} = 45 \pm 9$, $\delta_\perp = 23 \pm 5$
S_1-2	$g_{\|\|} = 1.97 \pm 0.126$, $g_\perp = 2.32 \pm 0.126$	$A_{\|\|} = 131 \pm 26$ $A_\perp = 45 \pm 9$	$\delta_{\|\|} = 40 \pm 8$, $\delta_\perp = 40 \pm 8$
S_1-3	$g_{av} = 2.18 \pm 0.126$	$A_{av} = 160 \pm 8$	$\delta = 180 \pm 36$
T_2			
S_2-1	$g_z = 2.02 \pm 0.1$, $g_x = 2.392 \pm 0.1$ $g_y = 2.35 \pm 0.1$		$\delta_z = 30 \pm 6$, $\delta_x = 35 \pm 9$ $\delta_y = 32 \pm 7$
S_2-2	$g_z = 2.191 \pm 0.1$, $g_x = 2.086 \pm 0.1$, $g_y = 2.066 \pm 0.1$		$\delta_z = 30 \pm 6$, $\delta_x = 18 \pm 4$ $\delta_y = 18 \pm 4$
S_2-3	$g_z = 2.005 \pm 0.1$, $g_x = 2.2 \pm 0.1$ $g_y = 2.162 \pm 0.1$		$\delta_z = 12 \pm 2.5$, $\delta_x = 30 \pm 6$ $\delta_y = 30 \pm 6$
S_2-4	$g_{\|\|} = 2.009 \pm 0.1$, $g_\perp = 2.13 \pm 0.1$		$\delta_{\|\|} = 12 \pm 2.5$, $\delta_\perp = 12 \pm 2.5$
T_3			
S_3-1	$g_{\|\|} = 2.011 \pm 0.1$, $g_\perp = 2.22 \pm 0.1$	$A_{\|\|} = 79 \pm 12$ $A_\perp = 38 \pm 6$	$\delta_{\|\|} = 18.4 \pm 3$, $\delta_\perp = 27 \pm 4$
S_3-2	$g_{\|\|} = 2.0275 \pm 0.1$, $g_\perp = 2.19 \pm 0.1$	$A_{\|\|} = 67 \pm 10$ $A_\perp = 38 \pm 6$	$\delta_{\|\|} = 15 \pm 2.25$, $\delta_\perp = 20 \pm 3$
S_3-3	$g_{\|\|} = 2.018 \pm 0.1$, $g_\perp = 2.18 \pm 0.1$	$A_{\|\|} = 71 \pm 11$ $A_\perp = 38 \pm 6$	$\delta_{\|\|} = 10 \pm 1.5$, $\delta_\perp = 15 \pm 2.25$

the $\mathbf{T_1}$ and $\mathbf{T_2}$ targets. The optimal values are found in a rather broad range of the values (from 0.5 to 0.9). In the case of the $\mathbf{T_3}$ test spectrum, however, the optimal area is rather narrow and is shifted toward $p_{crs} \sim 0.6$. The crossover probabilities larger than 0.7−0.8 or smaller than 0.4 distinctly deteriorate the performance. The optimal ranges for the mutation probabilities are more confined in comparison to the crossover ones. Large ($p_{mut} > 0.03-0.02$) and very small ($p_{mut} < 0.005$) rates become detrimental quite rapidly. For all test spectra the advantageous values appear in the vicinity of 0.01. Comparison of the operator performance maps for all investigated targets shows that the area of the optimal rates distinctly shrinks on passing from $\mathbf{T_1}$ to $\mathbf{T_2}$ and then $\mathbf{T_3}$. This indicates that targets with rather diverse components, like that of $\mathbf{T_1}$, imply a more open space of the probability rates than those composed of similar objects ($\mathbf{T_3}$).

The results of the sensitivity studies for the crossover and mutation operators revealed a rather strong dependence of the GA performance on the assumed probability values and on the nature of the investigated target. The mutation rates around 0.01 and the crossover rates in the range 0.5−0.7 appeared to be optimal settings for further investigations.

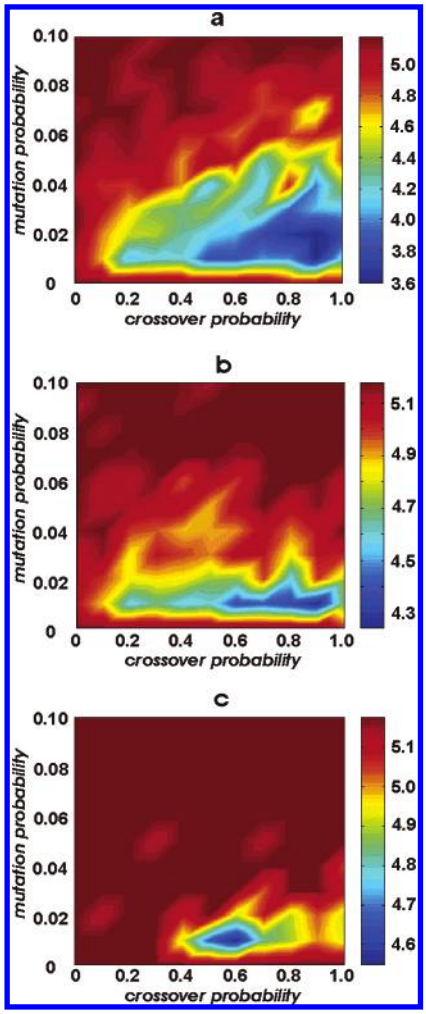

Figure 3. Operator performance maps for parametric sensitivity of the GA convergence as a function of the mutation and crossover probabilities for the $\mathbf{T_1}$, $\mathbf{T_2}$, and $\mathbf{T_3}$ targets. The color coding displays the convergence efficiency, gauged by the number of simulations required to achieve the INF threshold of 95% in the log scale, averaged over three independent runs. The shading has color resulting from bilinear interpolation of the colors at its four vertices.

5.2. Optimization of the Population Size. In general this parameter should be determined according to the complexity of the problem, and usually it is necessary to try out a range of the m values. We have investigated this issue in more detail on the same test data sets as above. The size of the population was systematically varied from 30 to 1000, while all other parameters were kept constant at $p_{crs} = 0.5$ and $p_{mut} = 0.01$. Generally the simulation success averaged over 10 runs and measured by the number of simulations required to pass the criterion of INF > 95% exhibited a moderate dependence on the population size with rather broad minima appearing at $m = 250$, 150, and 200 for the $\mathbf{T_1}$, $\mathbf{T_2}$, and $\mathbf{T_3}$ targets, respectively. However, for small sizes of the population, when the gene pool was probably insufficient, the results were quite scattered indicating strong dependence of the performance on the starting point. This was especially apparent in the case of the $\mathbf{T_1}$ and $\mathbf{T_2}$ test spectra composed of diverse EPR signals. In contrast, for the $\mathbf{T_3}$ spectrum being a superposition of the signals similar in shape, the scattering of the results was more uniform and the optimum in the population size better pronounced. Eventually, the selection of the initial population size appeared less crucial than the selection of the crossover and mutation rates, and for further investigations the values within the range of 150−250 were used.

Table 3. Values of the Genetic Algorithm Parameters Used in Numerical Experiments with the $\mathbf{T_1}$, $\mathbf{T_2}$, and $\mathbf{T_3}$ Test Spectra

GA parameter	$\mathbf{T_1}$	$\mathbf{T_2}$	$\mathbf{T_3}$
population size	200	150	250
maximum number of generations	750	1000	600
crossover probability	0.9	0.6	0.6
crossover type	uniform	uniform	uniform
mutation probability	0.02	0.01	0.01

6. OPTIMIZATION OF EPR SPECTRA

6.1. Simulated Data. The best way to evaluate the efficiency of an optimization routine is to fit a spectrum with a priori known parameters (a simulated spectrum). Only in such cases a complete agreement between the calculated and fitted spectra can be obtained, identifying the global minimum univocally. In this study we compared the performance of the Powell, GA, and the hybrid GA-Powell optimization methods, by following the evolution of convergence for the noiseless $\mathbf{T}_i$, $i = 1, 2, 3$ test spectra, and for the same spectra contaminated with a white noise of SNR = 35 dB. These latter spectra are labeled hereafter as n-$\mathbf{T}_i$. The signal-to-noise ratio was defined as follows

$$\mathrm{SNR} = 10\log a_{\max}^2/\sigma^2 \qquad (10)$$

where a_{max} and σ are the maximum values of the signal amplitude and the variance of the added noise, respectively.[27] For the convergence tests an uncertainty limit of ±20% was imposed on all adjustable parameters, whereas the starting point was selected at random. Twenty trials were effected for the Powell method, and 10 independent initializations of the genetic algorithm were used to equilibrate the results. The average RMS value corresponding to the INF of 95% was determined empirically for all test spectra, by fitting the plot RMS vs INF to a logarithmic curve (RMS = $a$ln-[INF] + b). The values of the GA parameters used in the numerical experiments are collected in Table 3.

The performance profiles for the noiseless $\mathbf{T}_1$, $\mathbf{T}_2$, and $\mathbf{T}_3$ spectra are shown in Figure 4. For these data exact solutions (RMS → 0) are in principle possible. From comparison of parts a and b of Figure 4 it is clear that for the $\mathbf{T_1}$ target the Powell method markedly outperformed GA, out of 20 trials 12 reached the INF level in less than 3000 simulations. Among them, in 3 cases a perfect fit (global minimum) was achieved, whereas the remaining 9 runs were caught in some local minima yet below the INF threshold. However, in 8 cases a complete failure was observed, demonstrating an obvious sensitivity of the direct search on the starting point. The analogous progress of the convergence for the GA optimization was distinctly slower but clearly more proficient. All 10 runs converged below the INF limit, albeit in a few cases it required more than 7000 simulations. The decrease in RMS was approximately exponential in nature, suggesting that the most rapid improvements occurred early in the evolutionary process. The obtained final GA fits were always worse than those observed in the most successful runs of the Powell algorithm.

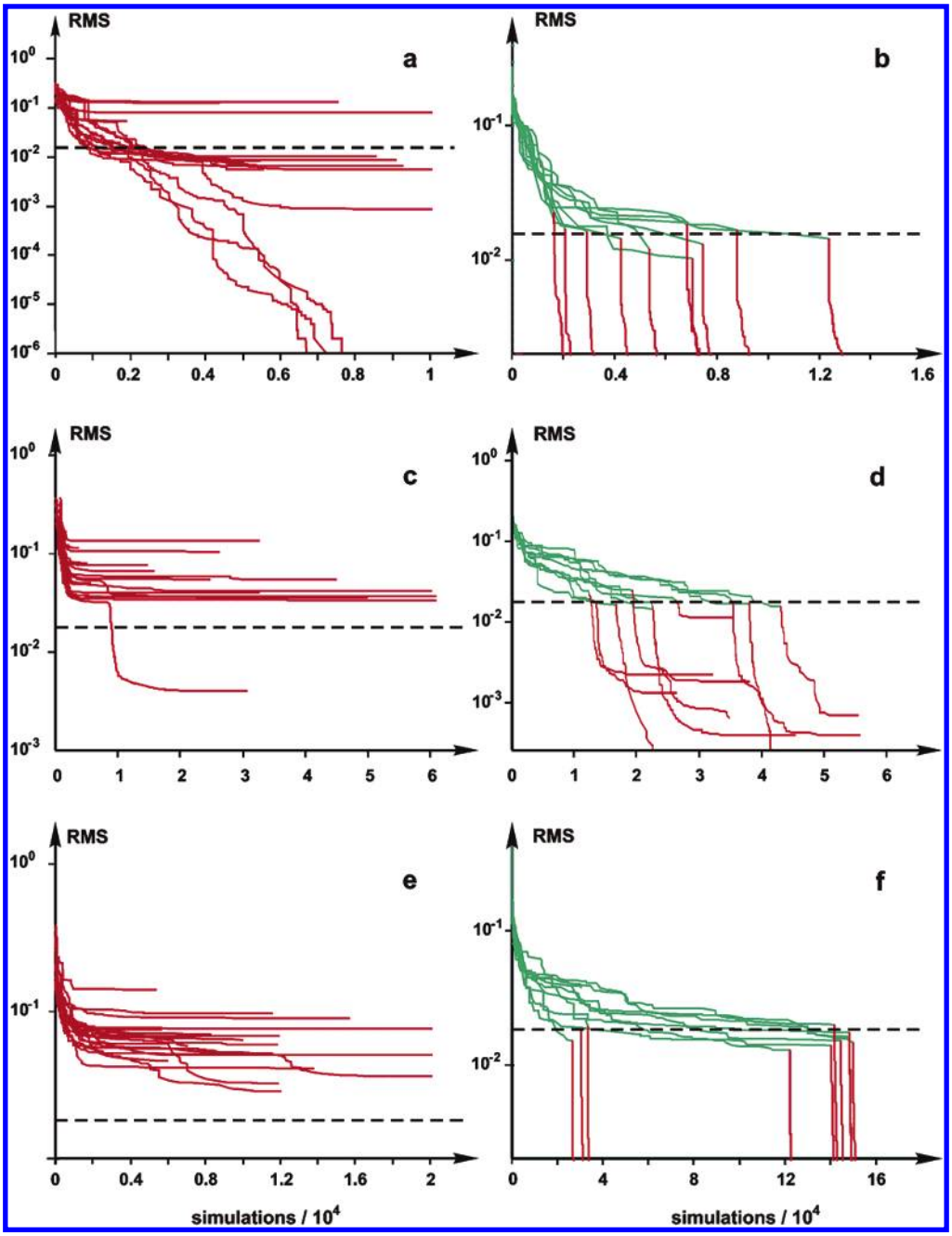

Figure 4. Performance profiles for the Powell (a, c, e) and the GA (green lines) combined with the Powell (red lines) optimization of the noiseless $\mathbf{T_1}$, $\mathbf{T_2}$, and $\mathbf{T_3}$ test spectra (b, d, f). The horizontal dashed line indicates an average RMS value corresponding to INF of 95% (see the text for more details).

For the more demanding $\mathbf{T_2}$ spectrum the situation changed dramatically (Figure 4c,d). While the slow decent of RMS in the genetic algorithm optimization demonstrated clearly that the overall quality of the fit was steadily improved as the population evolved, in the case of the Powell method only for one fortuitous run a satisfactory suboptimal solution was achieved. All other attempts became essentially stacked in various shallow minima situated distinctly above the assumed INF level, already at quite early stages of the optimization process. Further prolongation of the optimization course was completely inefficient (Figure 4c) in contrast to GA that showed a moderate but persistent progress, satisfying the INF criterion in all runs (Figure 4d). This superlative behavior of GA was further magnified on passing to the most congested spectrum $\mathbf{T_3}$. While the Powell method completely failed in this case, with the genetic algorithm the INF limit was achieved in most attempts. However, the final fits were clearly not optimal, as it can be judged from the terminal RMS values (Figure 5e,f). Thus, the test experiments have revealed an expected robustness of the global GA search and its inherent difficulty in fine refinement. For improvement of the optimization efficacy the genetic algorithm search was next hybridized with the Powell method.

The performance of the hybrid GA-Powell algorithm is shown in Figure 4b,d,f. After running the genetic algorithm optimization, once the convergence approached the INF limit, the current values of the adjustable parameters were taken as the starting point for the subsequent Powell refinement, following the flowchart shown in Figure 1. Spectacular convergence, leading to a practically perfect fit observed for the $\mathbf{T_1}$ and $\mathbf{T_3}$ test spectra, revealed that GA can very

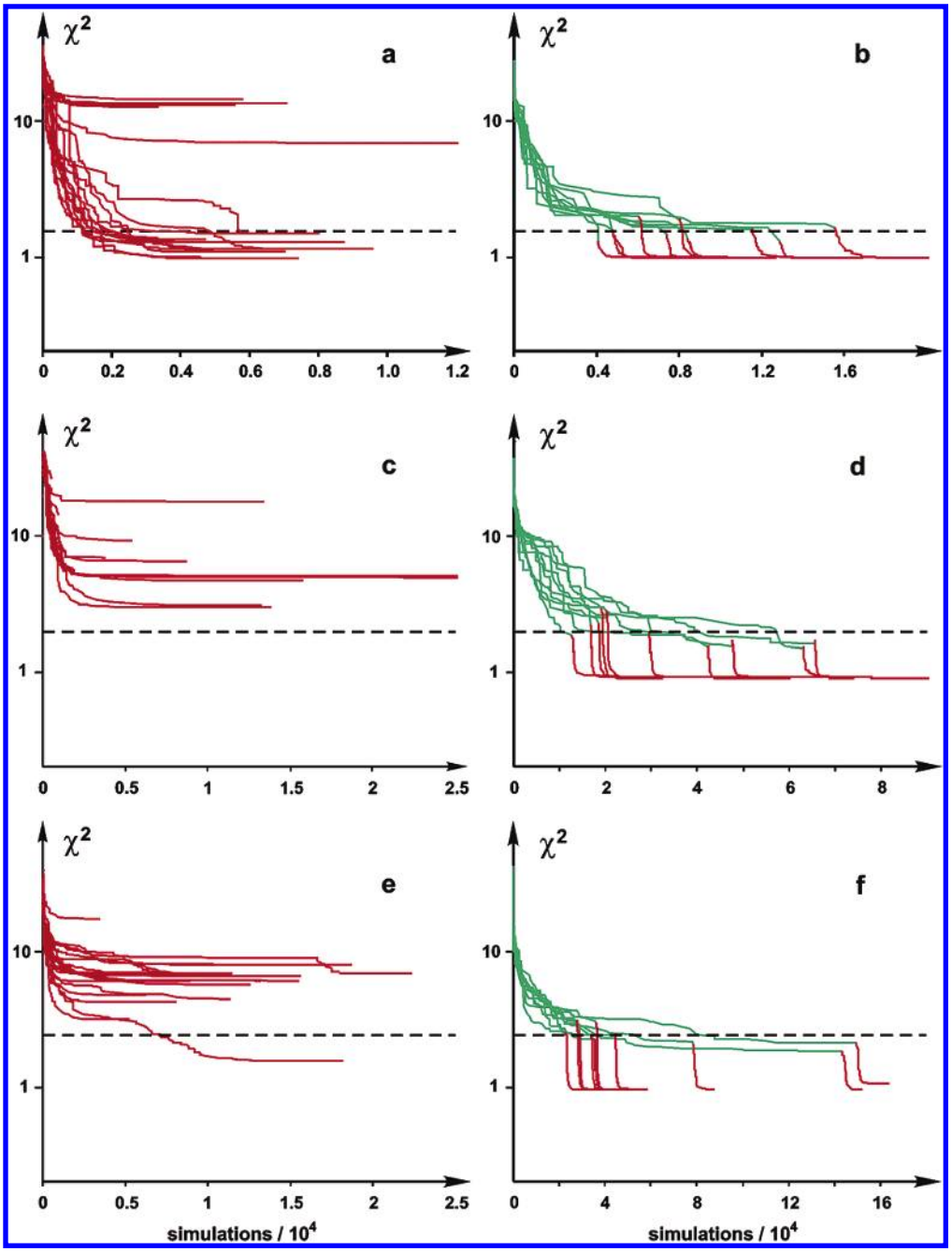

Figure 5. Performance profiles for the Powell (a, c, e) and the GA (green lines) combined with the Powell (red lines) optimization of the noisy n-$\mathbf{T_1}$, n-$\mathbf{T_2}$, and n-$\mathbf{T_3}$ test spectra (b, d, f). The horizontal dashed line indicates an average RMS corresponding to INF of 95% (see the text for more details).

effectively locate promising regions in the search space that are close to the global minimum. However, in the case of the $\mathbf{T_2}$ spectrum the performance of the hybrid approach was clearly deteriorated as the global minimum was located only twice. Most of the subsequent Powell refinements became confined in various suboptimal regions of the H_p space. However, the use of synthetic test spectra allows verifying the quality of the result by comparing the optimized parameters with their known input values used to generate the $\mathbf{T}_2$ spectrum (Table 4). The final adjusted values are given as the average over 10 runs of the hybrid algorithm together with their standard deviations. From the comparison of the adjusted parameters and the corresponding input values we can conclude that despite the suboptimal solution most of the optimized parameters agree well with the original values. The difficulty in reaching the global minimum for the $\mathbf{T_2}$ spectrum was apparently caused by the relatively large errors in determination of the σ_z line widths for the S_2-1 and S_2-4 signals. Indeed, both g_z-components being very weak are largely suppressed by the dominant g_z band of the S_2-2 signal (Figure 2b). As a result, contributing only slightly to the RMS value, they cannot be precisely determined.

The progress of convergence for the test spectra contaminated with the noise is shown in Figure 5. For the n-$\mathbf{T_1}$ spectrum, the Powell method with only 8 out of 20 successful trials significantly diminished its convergence efficiency in comparison to the noiseless $\mathbf{T_1}$ spectra (Figure 5a). Obviously location of the global minimum in the presence of the noise is a more difficult task. The performance of GA seems to be not much affected by the spectral noise as for most of

Table 4. Comparison of the Parameters Optimized with the Hybrid GA-Powell Method with the Known Input Values of the $\mathbf{T_2}$ Spectrum Averaged over 10 Runs

center	parameter	input values	averaged optimized values for n-$\mathbf{T_2}$	standard deviation
$\mathbf{S_2}$-1	*abundance*	0.100	0.099	0.002
	g_z, g_x, g_y	2.020, 2.392, 2.350	2.016, 2.390, 2.348	0.003, 0.001, 0.001
	$\delta_z, \delta_x, \delta_y$/G	30.0, 35.0, 32.0	29.7, 37.9, 30.3	2.2, 0.3, 1.1
$\mathbf{S_2}$-2	*abundance*	0.500	0.499	0.01
	g_z, g_x, g_y	2.191, 2.086, 2.066	2.196, 2.080, 2.072	0.006, 0.010, 0.010
	$\delta_z, \delta_x, \delta_y$/G	30.0, 18.0, 18.0	28.9, 17.9, 18.0	1.7, 0.04, 0.04
$\mathbf{S_2}$-3	*abundance*	0.250	0.256	0.007
	g_z, g_x, g_y	2.005, 2.200, 2.162	2.0050, 2.198, 2.1620	7×10^{-5}, 0.003, 2×10^{-4}
	$\delta_z, \delta_x, \delta_y$/G	12.0, 30.0, 30.0	11.3, 29.9, 30.5	0.1, 0.5, 0.4
$\mathbf{S_2}$-4	*abundance*	0.150	0.144	0.004
	$g_{\|\|}, g_\perp$	2.009, 2.130	2.022, 2.1300	0.01, 10^{-5}
	$\delta_{\|\|}, \delta_\perp$/G	12.0, 12.0	13.1, 11.9	0.9, 0.1

Table 5. Summary of the Performance of the Hybrid GA-Powell Method on $\mathbf{T_i}$ and n-$\mathbf{T_i}$ Test Spectra

	$\mathbf{T_1}$	$\mathbf{T_2}$	$\mathbf{T_3}$	n-$\mathbf{T_1}$	n-$\mathbf{T_2}$	n-$\mathbf{T_3}$
number of runs	10	10	10	10	10	10
best convergence speed[a]	1996	19580	35586	4719	13800	24490
worst convergence speed	12981	48957	158765	16812	66158	146247
average convergence speed	6174	33494	117433	9167	34436	52056

[a] Expressed as the number of the simulations.

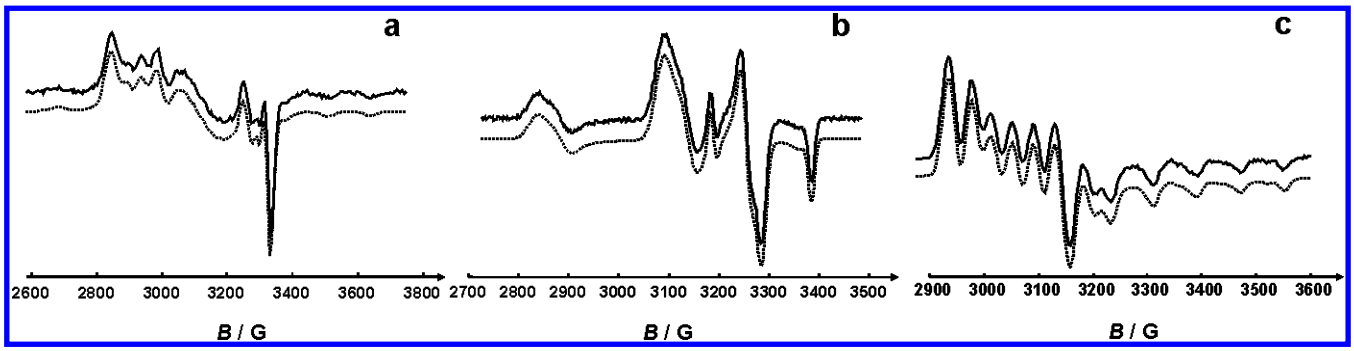

Figure 6. Comparison of the original and fitted n-$\mathbf{T_i}$ spectra: (a) n-$\mathbf{T_1}$, (b) n-$\mathbf{T_2}$, and (c) n-$\mathbf{T_3}$. Solid line indicates original spectrum and dotted line fitted spectrum.

the runs the INF limit was achieved, within the number of the simulations comparable to that of $\mathbf{T_1}$. In the case of n-$\mathbf{T_2}$ and n-$\mathbf{T_3}$ spectra the evolution of the fitness was quite similar (Figure 5b−f). The Powell optimization after some rapid progress at the very beginning became quickly saturated, distinctly above the INF level of 95%. Although, for the n-$\mathbf{T_3}$ target an accidental success could be noted, it was most probably owing to a very fortuitous choice of the starting point. Again GA clearly surpassed the performance of the Powell method and in tandem with the Powell refinement optimal solutions (χ^2 close to 1) were always reached (Figure 5d,f). The comparison between the original and the fitted test spectra n-$\mathbf{T_i}$ is shown in Figure 6.

The outcomes of the hybrid optimization technique, shown in plots b, d, and f in Figures 4 and 5, exhibit high diversity regarding the number of simulations needed to accomplish the task. There are several possible reasons, acting in conjunction, that may lead to such a result. They include (*i*) complications of the error function arising from the first derivative nature of EPR spectra, (*ii*) complex structure of the search space, (*iii*) stochastic nature of GA, and (*iv*) scarce coherence between RMS and INF. Although precise evaluation of their particular relevance would require separate detailed investigations, being now in progress, a provisional phenomenological explanation of such behavior seems plausible, based on the inspection of Figures 4 and 5. The transition from GA to Powell optimization is controlled by the critical value of INF = 95%. It takes place within the region where RMS function exhibits a distinct plateau indicating saturation of the GA search efficiency. Since there is no strict functional dependence between RMS and INF, the threshold value of INF in subsequent runs may be achieved at distinctly different RMS values. The very flat shape of the RMS function in the mature stages of the global search implies that even small differences in the actual RMS values may easily translate into quite large changes in the number of the necessary simulations, while reaching the INF limit. In other words, the pronounced diversity of the results reflects an apparent unsteadiness of the system in selecting the moment of passing from global to local search, which because of the stochastic nature of GA and flattened RMS becomes widely scattered. Statistical evaluation of the optimization results for $\mathbf{T_i}$ and n-$\mathbf{T_i}$ test spectra is shown in Table 5.

6.2. Real Spectra. To test the GA-Powell hybrid approach on experimental data, fitting of the complex EPR spectrum $\mathbf{T_4}$ due to nickel carbonyl complexes was chosen as a case study (Figure 7a). Optimization of real spectra is more demanding not only because of the ubiquitous noise but also due to ambiguities of the baseline correction and other signal distortions, which are not accounted for by the simulation algorithm. Nonetheless, the result of a fully automated

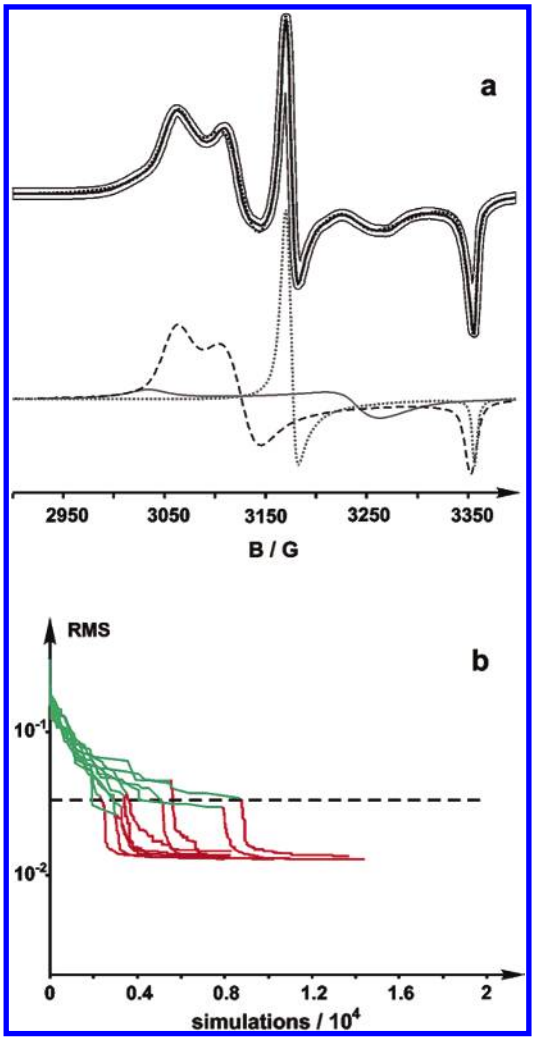

Figure 7. The best fit of the EPR spectrum $\mathbf{T_4}$ due to nickel carbonyl in ZSM-5, obtained with the hybrid GA-Powell optimization together with its INF envelope and the component signals (a) and progress of the fit with the number of simulations (b). The horizontal dashed line indicates an average RMS corresponding to INF of 95% (see the text for more details).

Table 6. Parameters of the Experimental $\mathbf{T_4}$ Spectrum Due to Nickel Carbonyl Complexes in ZSM-5 Zeolite, Determined Using the Hybrid GA-Powell Approach

center	parameter	averaged optimized values	standard deviation
$\mathbf{S_4}$-1	*abundance*	0.264	0.007
	g_z, g_x, g_y	2.081, 2.240, 2.090	0.004, 0.002, 0.002
	δ_z, δ_x, δ_y/G	49.6, 26.2, 37.2	6.3, 1.8, 0.5
$\mathbf{S_4}$-2	*abundance*	1.047	0.020
	g_z, g_x, g_y	2.0249, 2.2169, 2.1716	10^{-5}, 7×10^{-5}, 10^{-4}
	δ_z, δ_x, δ_y/G	9.8, 24.2, 28.1	0.8, 1.6, 1.7
$\mathbf{S_4}$-3	*abundance*	2.544	0.084
	$g_{\|\|}$, $g_\perp$	2.0224, 2.1392	6×10^{-5}, 10^{-5}
	$\delta_{\|\|}$, $\delta_\perp$/G	3.91, 9.80	0.09, 0.05

optimization using the hybrid approach, shown in Figure 7a, clearly demonstrates the power of the method, despite large uncertainties in the values of the starting parameters. The evolution of the convergence, for 10 independent runs (Figure 7b), gave practically the same results, but the number of the required simulations was clearly different, ranging from 2000 to 9000 in the extreme cases. This was caused by the different speed of GA, while moving toward the optimal solution depending on the starting point, since the subsequent Powell refinement was always quite rapid. The choice of the input parameters, however, was not crucial for achieving of the final success, influencing only the time of the optimization process. The results of the hybrid optimization of the spectrum $\mathbf{T_4}$ resolved into three components $\mathbf{S_4}$-1, $\mathbf{S_4}$-2, and $\mathbf{S_4}$-3 are collected in Table 6.

7. CONCLUSIONS

A simulation program has been developed to automate the entire process of determining the magnetic parameters and analysis of the powder EPR spectra. Genetic algorithm combined with Powell local optimization search provides a robust method for automated extraction of the parameters from experimental EPR spectra with minimum outside intervention. Owing to the combination of the exploitation and exploration processes, the genetic algorithm efficiently locates the most promising regions of the search space providing advantageous starting point for subsequent Powell refinement. The efficiency of the method was demonstrated using synthetic and real multicomponent test spectra of various complexities. The ranges of the optimized parameters do not need to be narrow, so knowledge of the accurate starting values is not necessary. The results reported here augur well for future successful applications of the hybrid approach to determine the parameters of complex powder EPR spectra.

ACKNOWLEDGMENT

This work was supported by the Committee for Scientific Research of Poland, KBN, as the Research Project number 3 T09A 147 26.

REFERENCES AND NOTES

(1) Abragam, A.; Bleaney, B. *Electron Paramagnetic Resonance of Transition Ions*; Clarendon Press: Oxford, 1970.
(2) Pilbrow, J. R. EPR spectroscopy of poorly characterized systems: a historical and current view. *Appl. Magn. Res.* **1994**, *6*, 161−181.
(3) Mubbs, F. E.; Collison, D. *Electron Paramagnetic Resonance of d Transition Metal Compounds*; Elsevier: Amsterdam, 1992.
(4) Eldershaw, C. *Report on Determination of Spin Hamiltonian Parameters from Electron Paramagnetic Resonance Spectra Using Numerical Nonlinear Optimization Methods*; The University of Queensland, Australia, 1996.
(5) Misra, S. K. A Rigorous Evaluation of Spin-Hamiltonian Parameters and Line width from a Polycrystalline EPR Spectrum. *J. Magn. Reson.* **1999**, *140*, 179−188.
(6) Fajer, P. G.; Bennett, R. L. H.; Polnaszek, C. F.; Fajer, E. A.; Thomas, D. D. General Method for Multiparameter Fitting of High-Resolution EPR Spectra Using a Simplex Algorithm. *J. Magn. Reson.* **1990**, *88*, 111−125.
(7) Kirkpatrick, S.; Gelatt, C. D.; Vecchi, M. P. Optimization by simulated annealing. *Science* **1983**, *220*, 671−680.
(8) Goldberg, D. E. *Genetic Algorithms in Search, Optimization, and Machine Learning*; Addison-Wesley: New York, 1989.
(9) Davis, L. *Handbook of Genetic Algorithms*; Van Norstrand Reinhold: New York, 1991.
(10) Bernhard, W. A.; Fouse, G. W. Simulation of Powder ESR Spectra of Organic Free Radicals. *J. Magn. Reson.* **1989**, *82*, 156−161.
(11) Griffin, M.; Muys, A.; Noble, C.; Wang, D.; Eldershaw, C.; Gates, K. E.; Burrage, K.; Hanson, G. R. XSOPHE, a Computer Simulation Software Suite for the Analysis of the Electron Paramagnetic Spectra. *Mol. Phys. Rep.* **1999**, *26*, 60−84.
(12) Lucasius, C. B.; Kateman, G. Understanding and Using Genetic Algorithms, Part 1. Concepts, Properties and Context. *Chemom. Intell. Lab.* **1993**, *19*, 1−33.
(13) Hibbert, D. B. Genetic Algorithms in Chemistry. *Chemom. Intell. Lab.* **1993**, *19*, 277−293.
(14) Adamski, A.; Spałek, T.; Sojka, Z. Application of EPR Spectroscopy for Eludidation of Vanadium Speciation in VO_x/ZrO_2 Catalysts Subject to Redox Treatment. *Res. Chem. Intermediat.* **2003**, *29*, 793−804.

(15) Filipic, B.; Strancar, J. Tuning EPR Spectral Parameters with a Genetic Algorithm. *Applied Soft Computing* **2001**, *1*, 83−90.
(16) Pilbrow, J. R. *Transition Ion Electron Paramagnetic Resonance*; Clarendon Press: 1990.
(17) Sojka, Z.; Che, M. EPR Techniques Applied to the Study of Chemistry and Catalysis on Oxide Surfaces. *Appl. Magn. Reson.* **2001**, *20*, 433−456.
(18) Weil, J. A. The Simulation of EPR Spectra: A Mini-Review. *Mol. Phys. Rep.* **1999**, *26*, 11−24, and references therein.
(19) Kriste B. Methods for Automated Analysis and Simulation of Electron Paramagnetic Resonance Spectra. *Anal. Chim. Acta* **1992**, *265*, 191−200.
(20) Fogel, L.; Owens, A.; Walsh, M. *Artificial Intelligence through Simulated Evolution*; John Wiley: 1966.
(21) (a) Rechenberg, I. *Evolutionsstrategie: Optimierung Technischer Systeme nach Prinzipien der Biologischen Evolution*; Frommann-Holzboorg: Stuttgart, 1973. (b) Schwefel, H.-P. *Numerical Optimization of Computer Models*; John Wiley and Sons: 1981.
(22) Holland, J. *Adaptation in Natural and Artificial Systems*; University of Michigan Press: 1975.
(23) Michalewicz, Z. *Genetic Algorithms + Data Structures = Evolution Programs*; Springer: Berlin, 1992.
(24) Davis, L. *Handbook of Genetic Algorithm*; Van Nostrand Reinhold: New York, 1991.
(25) Sojka, Z.; Stopa, G. Analysis of the Isotropic EPR Spectrum of $K_3[Cr(CN)_5NO]$. An Inorganic Chemistry Laboratory Experiment. *J. Chem. Educ.* **1993**, *70*, 675−678.
(26) Jong, A. K. D. *An Analysis of the Behavior of a Class of Genetic Adaptive Systems*, Ph.D. Thesis, University of Michigan, Ann Arbor, 1975.
(27) Choy, W. Y., Sanctuary, B. C. Using Genetic Algorithms with a Priori Knowledge for Quantitative NMR Signal Analysis. *J. Chem. Inf. Comput. Sci.* **1998**, *38*, 685−690.

CI049863S